Engineering Structures 116 (2016) 70–82

Contents lists available at ScienceDirect

Engineering Structures

journal homepage: www.elsevier.com/locate/engstruct

Stability of Statics Aware Voronoi Grid-Shells

D. Tonelli [a,*], N. Pietroni [b], E. Puppo [c], M. Froli [a], P. Cignoni [b], G. Amendola [d], R. Scopigno [b]

[a] University of Pisa, Department DESTeC, Pisa, Italy
[b] VCLab, CNR-ISTI, Pisa, Italy
[c] University of Genova, Department Dibris, Genova, Italy
[d] University eCampus, Via Isimbardi 10, 22060 Novedrate, CO, Italy

ARTICLE INFO

Article history:
Received 5 January 2015
Revised 6 December 2015
Accepted 29 February 2016

Keywords:
Grid-shells
Topology
Voronoi
Free-form
Imperfection sensitivity
Buckling
Equivalent continuum

ABSTRACT

Grid-shells are lightweight structures used to cover long spans with few load-bearing material, as they excel for lightness, elegance and transparency. In this paper we analyze the stability of hex-dominant free-form grid-shells, generated with the *Statics Aware Voronoi Remeshing* scheme introduced in Pietroni et al. (2015). This is a novel hex-dominant, organic-like and non uniform remeshing pattern that manages to take into account the statics of the underlying surface. We show how this pattern is particularly suitable for free-form grid-shells, providing good performance in terms of both aesthetics and structural behavior. To reach this goal, we select a set of four contemporary architectural surfaces and we establish a systematic comparative analysis between Statics Aware Voronoi Grid-Shells and equivalent state of the art triangular and quadrilateral grid-shells. For each dataset and for each grid-shell topology, imperfection sensitivity analyses are carried out and the worst response diagrams compared. It turns out that, in spite of the intrinsic weakness of the hexagonal topology, free-form Statics Aware Voronoi Grid-Shells are much more effective than their state-of-the-art quadrilateral counterparts.

1. Grid-shells: topology and stability

Grid-shells, also called lattice shells or reticulated shells, belong to the category of *lightweight structures*. The shape of these structures is optimized to support its own weight, its geometry being modified to provide additional stiffness to the overall structure.

Unfortunately, they are as efficient as exposed to risky buckling phenomena. In fact, in terms of structural behavior grid-shells are akin to shells but, at the same time, they are lighter and more flexible, hence even harder to analyze.

Shells typically suffer from modes interaction (i.e. some of the first linear buckling factors are coincident or have little separation) and imperfection sensitivity (i.e. a slight perturbation of their curvature may produce an unexpected deterioration of their static behavior). Both these phenomena are extremely detrimental and usually lead to a huge abatement of the theoretical linear buckling load of the perfect shell [2,3].

The same phenomena are usually less pronounced for grid-shells, although still present and indeed dangerous [4]. This is because the collapse load is more likely to be determined by limit point rather than by bifurcation of equilibrium.

In particular the grid-shell topology (together with the surface curvature) determines the ratio between extensional and inextensional internal strain energy, and thus the failure mode. For example Section 6.1 shows how usually an unstable symmetric bifurcation point appears in conjunction with triangular topology and quasi-funicular underlying surface with regular boundary, whereas limit points are usually associated with higher order topologies.

Analytical relationships are available for the calculation of the linear buckling load for shells of some shapes and restraint conditions [5], together with experimental knockdown factors for abating the linear unsafe values [6], as a result of the efforts of theoretical and industrial research carried out since the end of the XIX century. Unfortunately, no akin results are available for grid-shells.

Some attempts were done to evaluate the equivalent membrane stiffness and thickness of planar grids, in order to estimate the buckling load of grid-shells by using the available relationships for continuous shells [7,8]. Although overestimating the real buckling load and totally disregarding imperfections and material nonlinearity [9,4], the equivalent continuum method is very useful at least in the preliminary phase of the assessment process. Unfortunately, analytical solutions are available for a finite set of continuum shells, thus limiting its application. As a consequence, fully

* Corresponding author.
E-mail address: davide.tonelli@dic.unipi.it (D. Tonelli).

http://dx.doi.org/10.1016/j.engstruct.2016.02.049
0141-0296/

non-linear numerical analyses are the standard tool for the assessment of the stability of grid-shells.

From a geometrical point of view, grid-shells can be considered as the discretization of continuous shells: the continuous shape is tessellated by a set of connected piecewise linear modules composing a manifold mesh. It is evident that both curvature and meshing influence the statics of the structure, but while the effect of curvature can be somehow envisaged with the theory of shells [5], the outcome of meshing is much more difficult to predict and additionally few related studies are available [10, p. 239–244].

In summary, the behavior of a grid-shell is utterly affected by the *Gaussian curvature* of its underlying surface, the *grid topology*, the *grid spacing*, the *beam cross section*, the *joint stiffness* and the (potential) *stiffening method* [11,4].

Up to now, many examples of glass covered grid-shells have been built, the vast majority of which being designed with triangular and quadrilateral grid topologies [12–14]. Triangular grid-shells are unanimously credited as the most statically efficient structures as they rely on extensional deformation only, whereas quadrilateral grid-shells provide a better trade-off between statics efficiency, transparency and manufacturing cost. In fact, quadrilaterals achieve high transparency at equal weight, as their *area/perimeter* ratio is higher than that provided by triangles. Additionally, planar panels can be easily obtained that, by virtue of their almost right angles, are easier and cheaper to produce than triangular panels [15,16]. Unfortunately, quadrilateral and polygonal patterns generally undergo inextensional deformation (i.e. that involves beams bending), that makes them less efficient than their triangular competitors. As a consequence, most frequently the effective use of the quadrilateral topology required the adoption of special stiffening methods (e.g. bracing cables) [17], whereas higher order topologies such as the hexagonal are yet highly mistrusted by structural engineers. This attitude is not totally fair because while hexagonal grids display an isotropic equivalent mechanical behavior, quadrilateral grids are orthotropic and it is demonstrated that their efficiency greatly varies with the loading direction, becoming even much worse than that of hexagons in the most unfavorable case [18]. This in turn indicates that a grid-shell with an optimized Voronoi-like topology (i.e. hex-dominant) might display a very satisfying structural behavior.

In this paper we focus on pinning down the structural behavior of Statics Aware Voronoi Grid Shells introduced in [1], that are actually polygonal hex-dominant grid-shell structures, i.e. composed of mostly hexagonal faces, including a few generic polygonal faces, usually heptagons, pentagons and quads. From a purely geometric viewpoint, this kind of structures turns out to be extraordinarily *adaptive* and suitable for *free form architecture*, definitely much more than purely hexagonal structures [19]. In the following, we demonstrate how this pattern can be successfully used to tessellate *highly free form surfaces* providing static performances that are considerably better than current practice quadrilateral remeshing schemes, while for quite *regular* geometries the performances are comparable. This also demonstrates how the *'statics awareness'* introduced in [1] can be adopted to overcome the intrinsic structural weakness of polygonal topologies.

For the sake of brevity in the proposed experiments we considered no stiffening method (e.g. bracing cables). As a consequence all the beams' joints have been modeled as rigid (see Section 5.1 for more details).

2. Stability checks for grid-shells

Grid-shells are compressive structures and consequently they can display several types of stability failure [4,20]:

1. **member buckling:** the classic Euler beam buckling under concentric axial load;
2. **node instability:** a set of beams fails locally due to the snap through of a node;
3. **line instability:** all nodes of a ring in a dome or a generatrix of a barrel vault buckle simultaneously (less determinant for free-form shapes);
4. **global instability:** the whole structure undergoes sudden long-wave displacements.

Usually member instability is decisive for high grid spacing values (see Section 5.2 for a coherent definition of grid-spacing), whereas global instability and line instability are more likely to appear in conjunction with dense networks [4]. However, instabilities of type 1, 2 and 3 cannot be observed by using simple cells, simplified static schemes or the equivalent continuum method. Therefore, in the general case, the assessment of the load bearing capacity of a grid-shell relies on performing numerical non-linear buckling analyses: the so called 'direct' method. In particular, the Finite Element Analysis (FEM) proves to be very effective as it allows to:

- analyze any shape, also free-form shapes;
- point out buckling of all types;
- take into account the effect of imperfections;
- observe the softening behavior (geometrical non-linearity);
- introduce material non-linearity.

Therefore we performed systematic geometrically non-linear analyses with a commercial FEM software [21]. Details are given in Section 5.1. In particular, we chose not to consider material non-linearity because of the higher computational time needed and the large number of analyses performed. Indeed it is likely that the failure mode of grid-shells, especially if free-form, would be affected by yielding of the beams material (as is the case for the British Museum Great Court roof, for example). But the purpose of this study is not that of assessing the real buckling load of a grid-shell, but rather only that of estimating the buckling strength of the Statics Aware Voronoi Grid-Shells in comparison with their state-of-the-art competitors. For this reason, we have deemed geometrically non-linear analyses to be accurate enough for our aim.

3. Imperfection sensitivity analysis

It is well-known that the solution of the generalized eigenvalue problem:

$$det(\mathbf{K}) = det(\mathbf{K}_e + \lambda \mathbf{K}_\sigma) = 0 \tag{1}$$

where $\mathbf{K}$ is the initial global stiffness matrix, $\mathbf{K}_e$ is the initial global elastic stiffness matrix, $\mathbf{K}_\sigma$ is the global geometric stiffness matrix and λ is the load factor that amplifies the external loads, provides an overestimate of the real buckling load. This is especially the case for shells and grid-shells endowed with a high level of symmetry, where imperfection sensitivity and modes buckling interaction may even halve the theoretical buckling load [3]. This happens because these kind of structures are characterized by a high membrane to bending strain energy ratio, and this in turn makes them very sensitive to imperfections [22]. The process of evaluating the effects of imperfections on the buckling strength of a structure is known as imperfection sensitivity analysis, and it is essential in assessing the safety of efficient structures.

Koiter [2] elaborated the 'initial post-buckling theory', which assumes that it is possible to evaluate the behavior of the imperfect structure by knowing the behavior of the perfect one. It applies to structures showing bifurcation of equilibrium and lays its foundations

on the asymptotical approximation of the post-buckling path. Unfortunately, it is limited to almost linear fundamental paths only as well as imperfections of small amplitude.

A more recent trend is the 'mimimum perturbation energy' concept, which identifies snap-through phenomena towards secondary equilibrium paths by perturbing the system [23,24].

Nevertheless, the most commonly adopted method for determining the effect of imperfections is that of numerically analyzing the imperfect model itself, which is called under the name of 'direct approach'. This in turn raises the question of how to compute the 'worst imperfection', i.e. that imperfection that yields the lower buckling factor. It is worth noticing that the problem of finding the worst imperfection shape within a given amplitude limit is also coupled in the variables shape and amplitude. This search is still an open problem and some even think it does not have a unique solution [25]. Indeed this approach has the advantage that complex searches for the non-linear post-critical path are avoided, as the introduction of the imperfections converts bifurcation points into limit points. On the other hand, it is definitely computationally expensive as it requires to carry out a series of fully non-linear analyses on a (possibly infinite) set of models adulterated with different imperfections. The computational cost is sometimes discouraging, especially for everyday design. As a consequence, several variations to the general procedure have been proposed.

Deml and Wunderlich [26] propose to describe imperfections as additional nodal degrees of freedom and to solve for both the buckling load and the corresponding 'worst' imperfection shape by solving an extended system of nonlinear equations.

After the studies of Ho [27] it was known that the worst imperfection shape is to be sought after within the convex linear combinations of the linear eigenmodes (i.e. the eigenvectors $\mathbf{u}_i$ associated to the solutions λ_i of Eq. (1), with $\mathbf{u}_i^T\mathbf{u}_j = \delta_{ij}$). Subsequently it was also observed that in certain cases, especially when the softening behavior is much pronounced in the pre-buckling phase, the worst imperfection shape must also take into account the non-linear eigenmodes (i.e. the eigenvectors $\mathbf{u}_i$ associated to the solutions λ_i of Eq. (1), with $\mathbf{K}$ being evaluated just before the bifurcation point) [28].

A modern approach of absorbing this knowledge is that of setting up a non-linear optimization problem in which the solution is sought within convex linear combinations of linear and non-linear eigenmodes, subjected to user-defined imperfection amplitude constraints, by minimizing the buckling load [29]. As expected, it is found out that lower buckling loads are obtained by considering also non-linear buckling modes and that the worst imperfection shape is usually composed of several eigenmodes. Additionally, it is noticed that the first non-linear eigenmode is a very good approximation of the worst imperfection shape. Nevertheless, it is also common knowledge that the first linear eigenmode represents a satisfactory approximation as well [30], although for some structures higher linear eigenmodes might erode the load bearing capacity even more [31].

Kristanic and Korelc [32] propose instead a linear optimization problem, by carefully choosing linear constraints on both the shape and the amplitude of the imperfections. They also include deformation shapes (i.e. the displacement fields of the structure due to relevant load cases) among the base shapes for the generation of the convex linear combinations.

However, other studies showed that the worst imperfection form depends on the specific combination of the structure's geometry and loading. Additionally dimples and local imperfections in general, that are more relevant to production and may also represent the occurrence of local instabilities along the loading path, might also cater for the maximum reduction in load bearing capacity [33,34]. Therefore, eigenmodes combinations as well as all long-wave imperfections may overestimate the buckling load. Additionally, it is worth noting that some authors include also several post-buckling deformed shapes among the competitors for the worst imperfection shape [33,35].

In the light of these results the concept of 'quasi-collapse-affine imperfection' has emerged, together with the awareness that the worst imperfection shape cannot be pinpointed [25]. Schneider finds that the worst imperfection pattern does not exist for shells because it depends on the imperfection amplitude. Additionally, it cannot be spotted as it relies heavily on clustering of instability loads, crossing of secondary equilibrium paths in the post-buckling range and material non-linearity. Therefore he introduces the concept of 'quasi-collapse-affine imperfections': displacement fields extracted from the initial stage of the buckling process, obtained by conveniently restricting the space of the shape functions. These imperfections turn out to be more unfavorable than eigenmodes, especially when the instability is caused also by material non-linearity. Actually they initiate the buckling process (they 'stimulate' it) thus allowing to approach the most unfavorable imperfection pattern [35].

Most of the described contributions are specific to shells, whereas few references specific to grid-shells are available. Bulenda and Knippers [20] propose to adopt as imperfection shapes the non-linear eigenmodes and the displacement shapes of the grid-shell under relevant load cases.

We use GSA as a FE-program [21], a commercial software which does not allow the user to check and manipulate the stiffness matrix. Thus we can neither obtain non-linear eigenmodes nor restrict the space of the shape functions in order to compute 'virtual' initial buckling shapes (as proposed by Schneider [35]). However, our study is a parametric analysis on the imperfection sensitivity of grid-shells with different topology (i.e., triangular, quadrilateral and hex-dominant), and not a thorough assessment of the safety of real projects. All this being said, we content ourselves with 'stimulating' the buckling process as proposed by Schneider [25,35], by adopting the following imperfections shapes (see Fig. 2 for an example):

1. the displacement shape obtained by linear static analysis, addressed with the acronym *LS* in the following;
2. the initial buckling shape obtained by geometrically non-linear analysis (i.e. the 'real quasi-collapse-affine' imperfection according to Schneider [25,35]), addressed with the acronym *NLS* in the following;
3. the first linear eigenmode and convex linear combinations of the first ten linear eigenmodes, addressed with the acronym *LB* in the following. No optimization procedure is established: the generic *i*-th buckling mode is only included when a visual resemblance is noticed with the non-linear initial buckling shape of the grid-shell (i.e. *NLS*).

It is once again worth noticing that, as this is a comparative analysis and not a real project, only the dead load case has been considered. No asymmetric load cases have been addressed, neither in the buckling analyses nor in the definition of the imperfection shapes.

For each dataset (see Table 1), for each topology and for each imperfection shape, we have created a range of imperfect models by varying both the norm of the imperfection and its sign. The norm is Euclidean $\left(\|\mathbf{e}\|_2 = \sqrt{\sum_i (e_{ix}^2 + e_{iy}^2 + e_{iz}^2)}\right)$ and it was sampled at regulars intervals $\pm[25020015010050250]$ mm. Every time the imperfections shapes have been scaled according to the selected maximum norm and added to the perfect geometry. We have also taken into account the sign of the imperfections, as it may significantly influence the buckling behavior of the grid-shell.

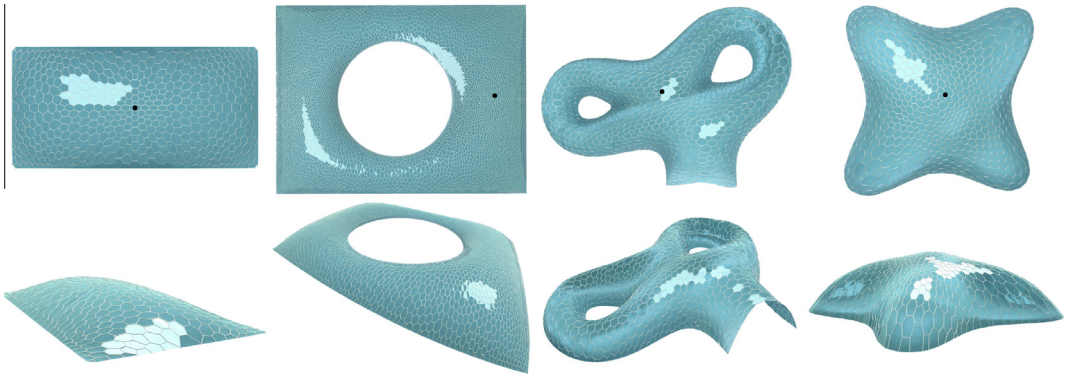

Fig. 1. All datasets. From left to right respectively: *Neumünster Abbey* glass roof, *British Museum* great court glass roof, *Aquadom* and *Lilium Tower* architectural free form shapes. The black bullet is the state parameter adopted in the geometrically non-linear analyses.

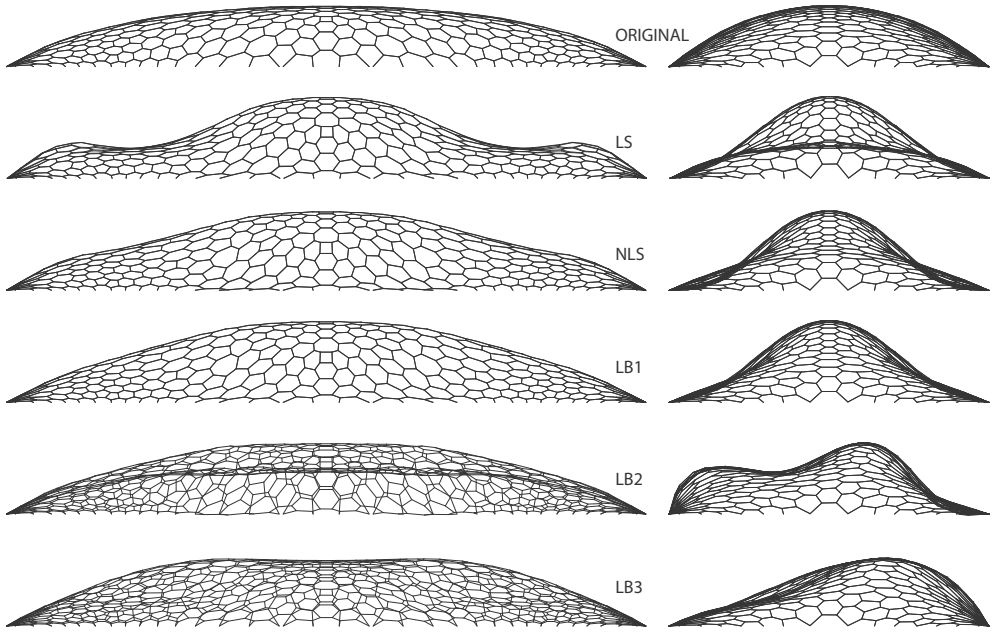

Fig. 2. Magnified deformed shapes for the hex-dominant remeshing of the Neumünster dataset, side and front views. From top to bottom respectively: ORIGINAL, LS, NLS, 1st LB eigenmode, 2nd LB eigenmode and 3rd LB eigenmode.

Table 1
Statistics on datasets. When a reference is given the remeshing comes from that source, otherwise it is a height field isotropic remeshing $s(x, y)$.

Dataset	Model	Vertices' valence	Vertices	Faces	Edges	Beams' section (mm)	Total length (m)
Neumünster Abbey	Triangular [39]	6	220	380	541	CS ϕ 60	966.7
	Quadrilateral	4	508	464	883	CS ϕ 60	932.7
	Voronoi	3	1076	553	1522	CS ϕ 60	956.9
British Museum	Triangular [40]	6	1746	3312	4878	CHS 120 × 30	10267.4
	Quadrilateral	4	4693	4452	8723	CHS 120 × 30	10184.8
	Voronoi	3	10,221	5784	14,829	CHS 120 × 30	10316.6
Aquadom	Quadrilateral [41]	4	1078	1001	1936	CHS 100 × 20	3672.1
	Voronoi	3	2382	1189	3400	CHS 100 × 20	3662.3
Lilium Tower	Quadrilateral [41]	4	665	636	1244	CHS 100 × 20	2139.9
	Voronoi	3	1432	717	2060	CHS 100 × 20	2121.1

In so doing, we ended up with a total of 13 imperfect models for each imperfection shape, for each topology and for each dataset, for a total of more than 400 models (see second column of Table 1). Each model has then been analyzed with the GSA FE-program [21], by carrying out geometrically non-linear buckling analyses (see Section 2 for reasons about neglecting material non-linearity and

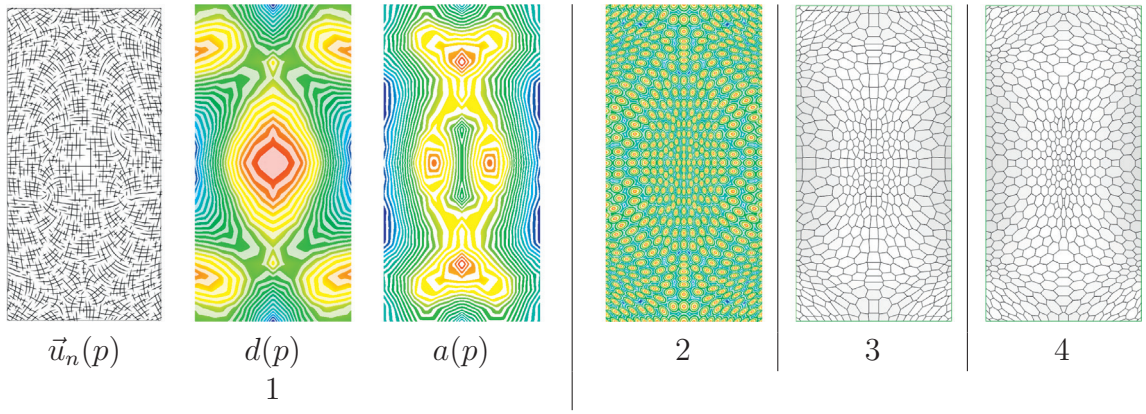

Fig. 3. The different steps composing the pipeline of [1]: the components of the stress tensor inducing the anisotropic metric (1); the distribution of seeds and their distance field (2); the corresponding ACVT (3); the final optimized tessellation (4).

Section 5.1 for details about modeling and load cases). Imperfection sensitivity diagrams are shown in Fig. 6, whereas relevant load–deflection diagrams are displayed in Fig. 7.

4. Statics Aware Voronoi Remeshing

Here we briefly report the method we use to design the Statics Aware Voronoi Grid-Shells. Our method is based on *Anisotropic Centroidal Voronoi Tessellations (ACVT)* [36] and it is driven by the statics of the input surface, aiming at improving the strength of the grid-shell as well as its aesthetics.

Voronoi diagrams appear in nature in many forms. In several cases, such as in the porous structure of animal bones, Voronoi-like structures optimize strength while keeping a light weight. We follow a similar approach to design hex-dominant grid-shells, by concentrating more cells of smaller size in zones subject to higher stress, while aligning the elements of our grid to the maximum stress direction. The pipeline of the method is summarized in Fig. 3 and briefly discussed below. The reader is referred to [1] for further details.

Given an initial surface Σ we first perform a linear static analysis of the continuous shell under dead load (although in theory every load condition can be adopted), thus obtaining a stress tensor for each point $p \in \Sigma$. As a thin shell can be considered in a plane stress condition, the resulting stress tensor is two-dimensional. Therefore we express it with respect to the local principal directions and we represent it as a pair of mutually orthogonal line fields[1] $\Psi(p) = (\vec{u}(p), \vec{v}(p))$, where $\vec{u}$ and $\vec{v}$ define the maximum and minimum principal stresses at each point of the surface, respectively. Since $\vec{u}$ and $\vec{v}$ are orthogonal, we decouple the scalar and directional information and represent Ψ as a triple $(\vec{u}_n(p), d(p), a(p))$, where $\vec{u}_n$ is a unit-length vector parallel to $\vec{u}, d = |\vec{u}|$ is the maximum stress intensity (henceforth called *density*), and $a = |\vec{u}|/|\vec{v}|$ is the *anisotropy* (see Fig. 3.1). Tensor Ψ induces an anisotropic metric $g_\Psi = \mathrm{diag}(\frac{1}{d^2}, \frac{a^2}{d^2})$ on surface Σ, where the matrix is expressed with respect to the principal reference system at p.

Next we compute a hex-dominant tessellation covering Σ, whose faces have a uniform distribution with respect to metric g_Ψ. Roughly speaking, this means that faces will be more dense where the maximum stress is higher and they will be elongated along the direction of maximum stress proportionally to anisotropy.

In order to do so, we sample a set of seeds on the surface [37], and then we relax their positions so that the distribution of seeds becomes uniform with respect to metric g_Ψ. Relaxation consists of computing the Voronoi diagram of the seeds under metric g_Ψ and iteratively moving each seed to the centroid of its Voronoi cell [38], until convergence. Note that, since g_Ψ has variable density and is anisotropic, the distribution of seeds will not be uniform with respect to the Euclidean metric: Fig. 3.2 depicts the distribution of seeds (red[2] dots) together with the corresponding field that encodes distance of points on the surface from the seeds; Fig. 3.3 depicts the corresponding ACVT, which assembles the (anisotropic) Voronoi cells of all seeds and is easily computed from the distance field.

Finally, we apply geometric optimization to improve the local shape of the faces of the hex-dominant mesh. Roughly speaking, we deform each face to its closest regular polygon under metric g_Ψ and we globally optimize the mesh by stitching adjacent polygons. The result of optimization is depicted in Fig. 3.4.

5. Experimental setup

We have tested our method on several input surfaces. Fig. 1 shows the rendered views of the hex-dominant remeshing of these surfaces (i.e. the Statics Aware Voronoi Grid-Shells), whereas Fig. 4 compares the top views of the various remeshings of each input surface. A summary of the datasets is presented in Table 1:

1. *Neumünster Abbey* is the glass roof of the courtyard of the Neumünster Abbey in Luxembourg, designed by RFR-Paris [39] and built in 2003.
2. *British Museum* is the great court glass roof in the British Museum: geometry rationalization by Prof. Chris J. K. Williams [40], structural design by Buro Happold and construction completed in 2000 by Waagner Biro.
3. *Aquadom* and *Lilium Tower* are architectural free form shapes; the latter is the top of the Lilium Tower skyscraper designed by Zaha Hadid architects. The quadrilateral remeshings for these datasets come from the statics optimization procedure of [41].

Neumünster and *British Museum* datasets represent lightweight, quite ordinary surface geometries and very low height-to-span ratio grid-shells, whereas *Aquadom* and *Lilium Tower* embody

[1] A line field is a vector field modulo its orientation: only the directions and sizes of $\vec{u}$ and $\vec{v}$ are relevant to Ψ, not their orientations.

[2] For interpretation of color in Figs. 3 and 8, the reader is referred to the web version of this article.

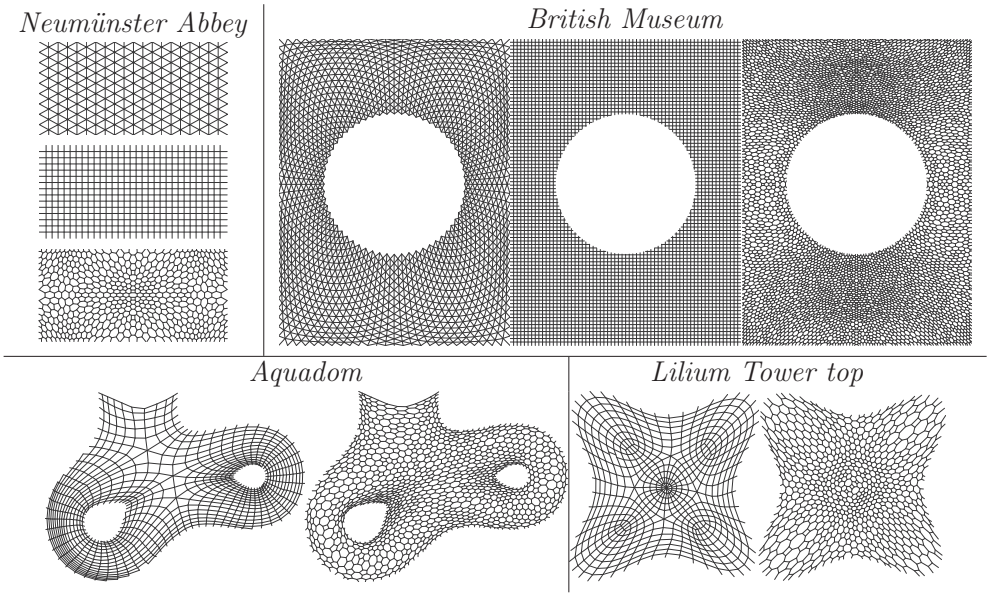

Fig. 4. Top views of all remeshings utilized in our comparative analysis.

architectural free form skins as well as high height-to-span ratio grid-shells.

5.1. Restraints, load conditions, numerical modeling

Since this is a comparative analysis and not a specific study on the topic of stability of grid-shells, some simplifications have been done:

1. All models have *pin joints* all over the boundary. This is a strong assumption as the boundary support can have a tremendous influence over the structure's behavior.
   The theory of bending of surfaces in the large proved that ovaloids (i.e. closed convex surfaces with positive Gaussian curvature everywhere) are rigid: i.e. they do not admit any infinitesimal bending except from motions [42]. Cohn-Vossen then proved that every ovaloid becomes non-rigid if any portion of it is removed [43–45]: i.e. it can undergo no more extensional deformation only but also inextensional deformation (i.e. bending).
   A shell, those with synclastic surface at least, can be regarded as a broken ovaloid whereas its restraints can be considered as devices aimed at restoring the surface continuity. It is evident that the higher the degree of restraint the more rigid the shell will be. Nevertheless, no clear relationship is available in literature relating the stiffness of a shell to its degree of restraint.
   Things may become even trickier for grid-shells, where variables like grid topology, grid-spacing and grid-orientation come into play. It is not a case that often the grid generation step takes the cue from both the boundary shape and the restraint condition. Just to cite a relevant example, the geometry of the British Museum triangular grid-shell has been generated with respect to a given specific support condition: i.e. sliding bearings together with tension beams along the edges, resisting the thust at the corners.
   All this being said, we understand that modeling a single type of restraint case does not allow us to study the relationship between grid-shell topology and restraint condition. We also understand that assuming a single unvaried support condition for all the models may put some of them at disadvantage, as their geometry often arises from a specific set of supports.
   Nevertheless we reckon that such a simplification is necessary due to the great amount of variables already involved in our analysis. Further studies will be required to address this topic.
2. The beams' joints are modeled as rigid.
3. The beams' size varies according to the specific model (as is shown in Table 1) but it is constant within each model.
4. The beams' cross section is always circular, either solid or hollow (see Table 1).
   The shape of the cross section determines the ellipse of inertia of the beam and hence its bending and torsional stiffnesses. While a triangular mesh resists in-plane shear mostly by means of extensional stiffness, the in-plane equilibrium of polygonal grids relies heavily on both bending and torsional stiffnesses of the mesh beams and hence in turn on the beams' cross section. This topic is thoroughly addressed and developed in [18], where the equivalent membrane stiffness, bending stiffness and thickness are analytically evaluated for the regular tilings of the Euclidean plane (i.e. isotropic triangular, quadrilateral and hexagonal grids).
   For the sake of this analysis, we have stuck to circular cross sections only because they are reasonably representative of the compact cross sections which are currently adopted in the design and construction of grid-shells [12–14,20];
5. The load is always uniformly distributed (i.e. dead load). Three load cases have been considered, respectively:
   (a) G_1 which is the dead load of the beams.
   (b) G_2 which is a uniform projected load of 0.75 kN/m^2 of magnitude, that stands for an hypothetical 25 mm thick glass coverage.
   (c) Q_k which is a uniform projected load of 1.00 kN/m^2 of magnitude, that represents the snow action.
   Then a serviceability load combination $q = 1.0G_1 + 1.0G_2\, m + 1.0Q_k$ is used to carry out all the analyses.
6. Material non-linearity is neglected as the analyses already involve many variables (see Section 2 for further explanations).
7. Each beam is modeled as a single finite element in order to reduce the computational time, while keeping an acceptable level of accuracy of the overall simulation. This simplification prevents form pointing out single member buckling, but it is still acceptable as member buckling is not the ordinary failure mode for grid-shells.

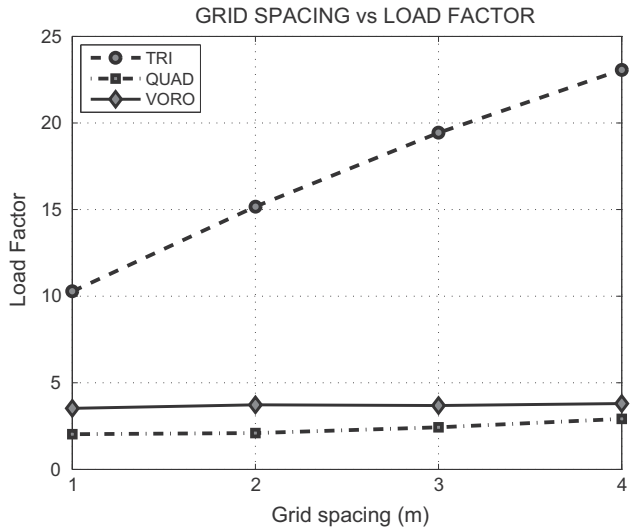

Fig. 5. Results of grid-spacing sensitivity analyses on a spherical cap surface (span-to-height ratio = 21.43). For this surface the triangular connectivity is the most sensitive to grid-spacing variations, as its load bearing capacity rockets as grid-spacing increases.

5.2. Statics comparison criteria

As we want to assess the structural performances of the Statics Aware Voronoi Grid-Shells, we set up a comparative evaluation with respect to other current practices (e.g. triangular and quadrilateral remeshing schemes).

As a basic criterion, equivalent grid-shells must be characterized by the same overall structural mass. Therefore in the following the total mass of the structure is considered constant.

Also, in order to minimize the number of variables involved, the shape of the members cross section must be kept constant for all the topologies.

Nevertheless, as roughly stated by Gioncu [4] and Malek [11], the structural performance of a grid-shell with fixed topology is not only affected by the total weight of its members but also by its grid-spacing. Giving a coherent definition of grid-spacing for grid-shells with different geometry and topology is not a straightforward matter though.

As a first attempt, for grid-shells with isotropic and equi-areal cells only, one could argue that the grid-spacing could be defined as the bare *edge length*. It is evident though that different topologies are characterized by different *area/perimeter* ratios. This in turn means that each topology requires a different total number of cells as well as an overall different total length of members to cover a given surface. Together with the aforementioned constraints of fixed overall structural mass and beams' shape, this definition of grid-spacing leads also to grid-shells with different members size.

Similarly and more generically, for isotropic but non equi-areal grid-shells (i.e. adaptive grids, whose cells area may vary locally), the *average edge length* might be assumed as a measure of the grid-spacing.

In order to check the consequences of such a definition of grid-spacing we set up a bespoke numerical experiment, whose results are shown in Fig. 5. A grid-spacing sensitivity analysis has been carried out on a shallow spherical cap (60 m of span and 2.8 m of height) remeshed with isotropic triangular, quadrilateral and Voronoi-like topology, respectively. Solid circular beams with tailored radia have been assigned to each remeshing in order to keep the total mass always constant.

The grid-spacing represented on the x-axis of the diagram is defined as the edge length for the isotropic triangular and quadrilateral topologies and as the average edge length for the Voronoi topology.

By increasing the grid-spacing the overall members length decreases, while the total mass is kept constant (see above).

Looking at the graph of Fig. 5 it is seen that the load factor varies with the grid-spacing. More importantly, the very gap in terms of load bearing capacity of grid-shells of different topology varies with the grid-spacing. This in turn means that the choice of an arbitrary grid-spacing (e.g. edge length) for our parametric studies on the buckling strength of grid-shells with different topologies would randomly affect the outcome of the experiments.

In light of these results we enforce the constancy of both total mass and total remeshing length as a sound criterion for generating 'statically equivalent' grid-shells with different topologies.

Therefore, concluding, two grid-shells with different topology share the same *overall grid-spacing* when they are characterized by the some total remeshing length.

6. Results

We have compared the triangular, quadrilateral and Statics Aware Voronoi-like patterns in terms of buckling strength, stiffness and imperfection sensitivity. In particular, the following comparisons have been performed:

Imperfection sensitivity analysis: this analysis shows how the buckling factor is affected by surface, grid-topology and imperfections shape, sign and amplitude (see Fig. 6 for results and Section 3 for the setup of imperfect models).
'Worst' response diagram *vs* **Grid-topology:** for each dataset (i.e. for each surface analyzed, see first column of Table 1) this study compares the 'worst' response diagram (i.e. that corresponding to the lowest load factor) of each grid-topology (see Fig. 7 for results – the state parameter on x axis represents the vertical deflection of the black bullet depicted in Fig. 1).
Response diagram *vs* **Imperfection amplitude:** this study outlines the variability of the response diagram with the signed magnitude of the (worst) imperfection shape (see Fig. 8 for results). For the sake of brevity, only the results concerning the triangular and Statics Aware Voronoi Remeshings of the *Neumünster* dataset are reported.

6.1. Comparative imperfection sensitivity analysis

Some theoretical background may help framing the results obtained into a more generic context. To this aim, Fig. 6(e) and (f) describe two kinds of critical points: an unstable symmetric bifurcation point and a limit point [46], respectively. A structure characterized by an unstable symmetric bifurcation point displays a decreasing critical load for whatever imperfection is applied to its geometry, no matter the type nor the magnitude. In jargon the curve describing the variation of the structures's critical load with the imperfection shape and magnitude is called two-thirds power law cusp (see [46] and Fig. 6(e)-right). On the other hand, a structure characterized by a limit point shows either an increase or a decrease of its buckling load according to the sign of the imperfection applied to it. This behavior is well summarized by the monothonic non-singular curve represented in Fig. 6(f)-right.

A quick inspection of these curves provides a satisfactory insight in the stability of the structure at hand. In fact, the stability behavior of most part of lightweight compressive structures such as grid-shells can be usually related to one of those curves.

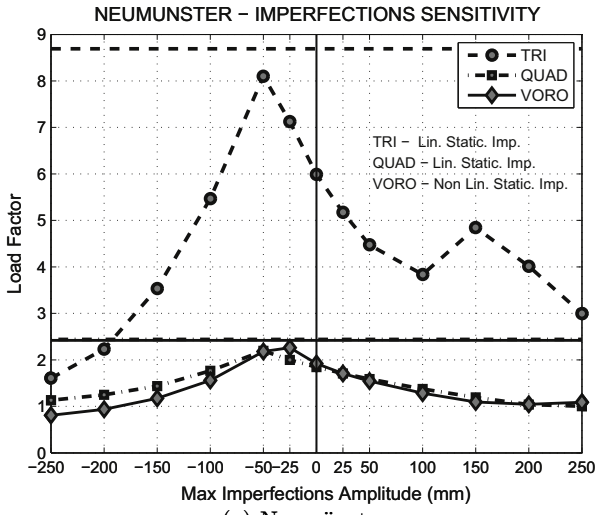

(a) Neumünster

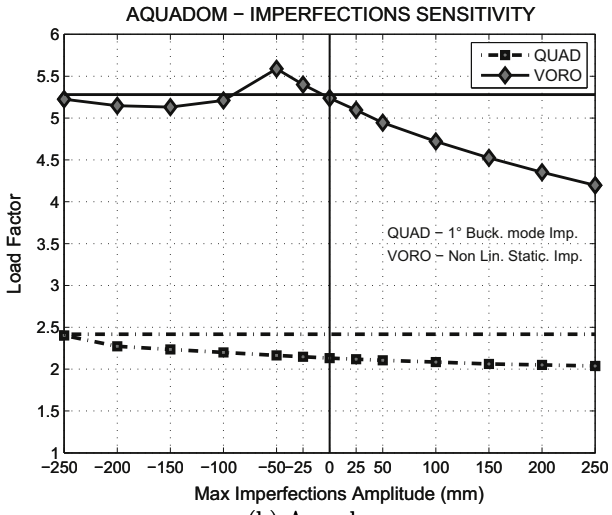

(b) Aquadom

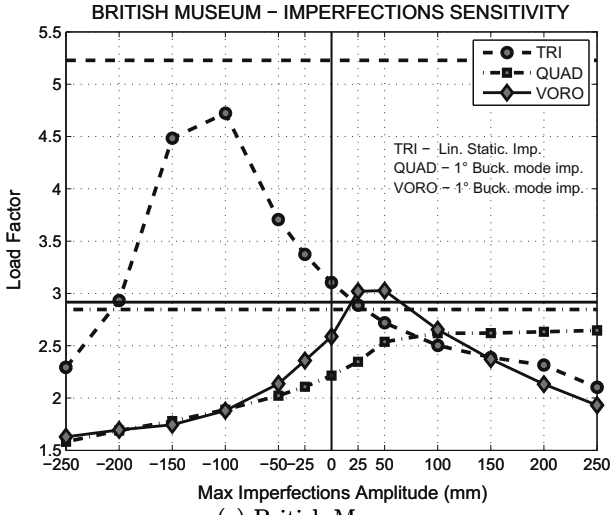

(c) British Museum

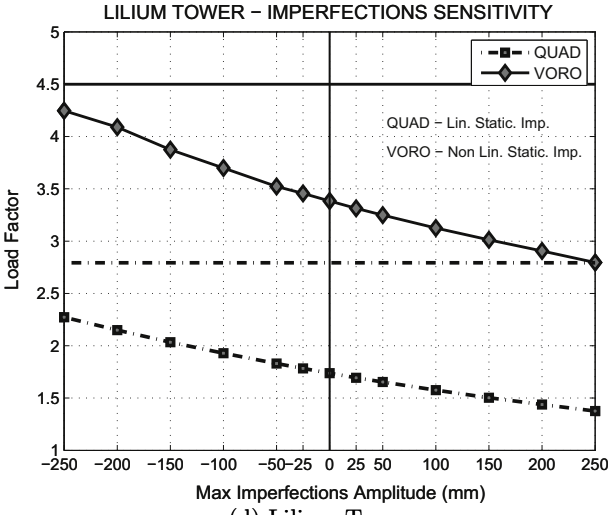

(d) Lilium Tower

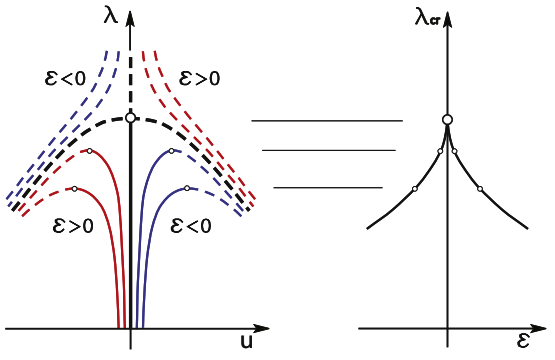

(e) Unstable symmetric bifurcation point

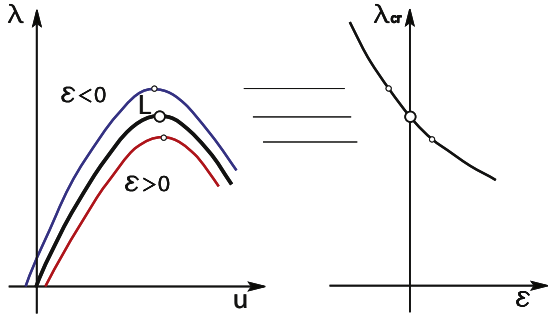

(f) Limit point

Fig. 6. Imperfection sensitivity results. On the left column, from top to bottom: *Neumünster Abbey* courtyard glass roof, *British Museum* great court roof and schematic representation of an unstable symmetric bifurcation point. On the right column, from top to bottom: *Aquadom*, *Lilium Tower* and schematic representation of a limit point. The horizontal lines in (a)–(d) represent the first linear eigenvalue (i.e. buckling load) computed on the corresponding perfect model. Text within the graphs of (a)–(d) recalls the 'worst' geometric imperfection shape which generates the graphs (see Section 3 for terminology).

Therefore we have graphed the outcome of our geometrically non-linear analyses in $\lambda - \varepsilon$ charts (i.e. critical load *vs* imperfection), in order to relate the various structural behaviors encountered to one of the aforementioned categories.

In accordance with Section 1, Fig. 6 shows that the triangular topology is definitely the most effective as well as the most sensitive to imperfections (see Figs. 6(a) and (c)), followed by our Statics Aware Voronoi Remeshing (Figs. 6(c) and (b)), while the quadrilateral

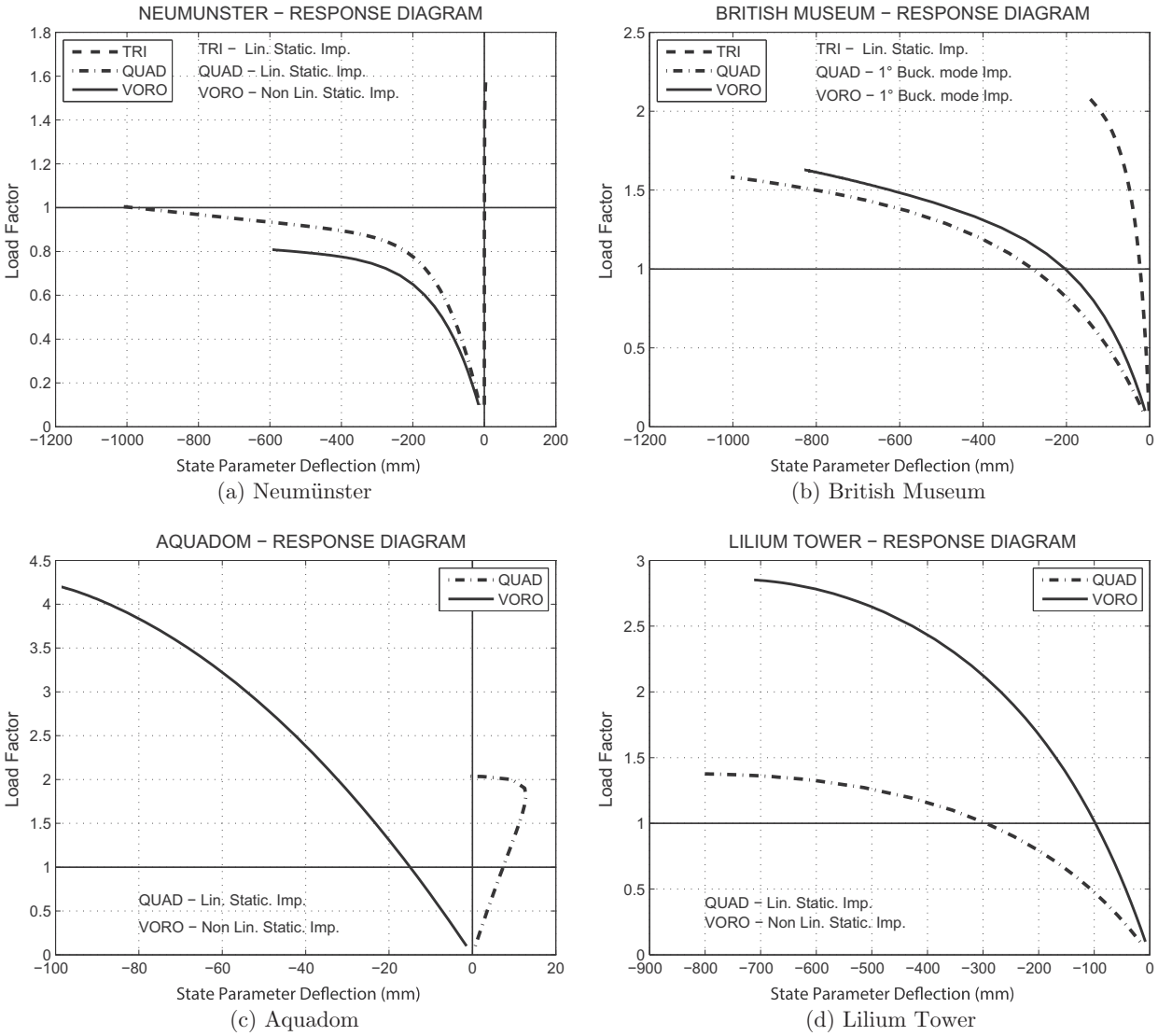

Fig. 7. 'Worst' response diagrams *vs* Grid-topology. Respectively from top left to bottom right: *Neumünster Abbey* courtyard glass roof, *British Museum* great court roof, *Aquadom* and *Lilium Tower* datasets. The horizontal solid lines represent the 'safety' unit load factor. Text within the graphs recalls the 'worst' geometric imperfection shape which generates the diagrams (see Section 3 for terminology). The state parameter referred to on the *x* axis is the vertical deflection of the black bullet depicted in Fig. 1.

pattern turns out to be the less sensitive to imperfections. These numerical results are in full accordance with the theoretical predictions of Tonelli [18], which where partially sketched in Sections 1 and 5.1.

Additionally, it is also evident that the regularity of the surface plays a central role in the definition of the critical point. According to Section 5, Neumünster and British Museum datasets represent rather regular geometries (the former more regular than the latter, see Figs. 1 and 4) whereas Aquadom and Lilium Tower Top are free-form surfaces. Figs. 6(a) and (c) show that the Neumünster and British Museum datasets display an *unstable symmetric bifurcation point* [46] (compare the graphs with the two-thirds power law cusp of Fig. 6(e)) roughly irrespective of the topology, although the trend is much more noticeable for the triangular topology. Similarly, Figs. 6(b) and (d) show that free-form surfaces such as Aquadom and Lilium datasets display a *limit point* [46] (compare the graphs with the monotonic non-singular curve of Fig. 6(f)), again irrespective of the topology.

Another clear result provided by Fig. 6 is that the Statics Aware Voronoi topology is just as efficient as the quadrilateral topology when the underlying surface is quite regular (Neumünster and British Museum datasets, respectively Figs. 6(a) and (c)) but its efficiency is even more than twice that of the quadrilateral pattern when the underlying surface becomes irregular or totally free-form (Aquadom and Lilium datasets, respectively Figs. 6(b) and (d)).

Contrary to polar-symmetric domes (which exhibit a symmetric graph both for negative and positive imperfections [20]), none of the tested grid-shells show a symmetric behavior with respect to the imperfection sign. Hence, the *sign of imperfections* plays a crucial role in the structural behavior of grid-shells. Besides, the singularity of the cusp representative of the unstable symmetric bifurcation point of Figs. 6(a) and (c) does never correspond to the perfect model. This in turn means that the perfect grid-shell does not necessarily produce the highest buckling factor (it never does in our experiments). Therefore, in certain circumstances, a slight imperfection acts as a mild stiffening for the grid-shell.

As a last remark, at least under dead load, the 'worst' imperfection shape is topology-dependent. It is seen that, among the

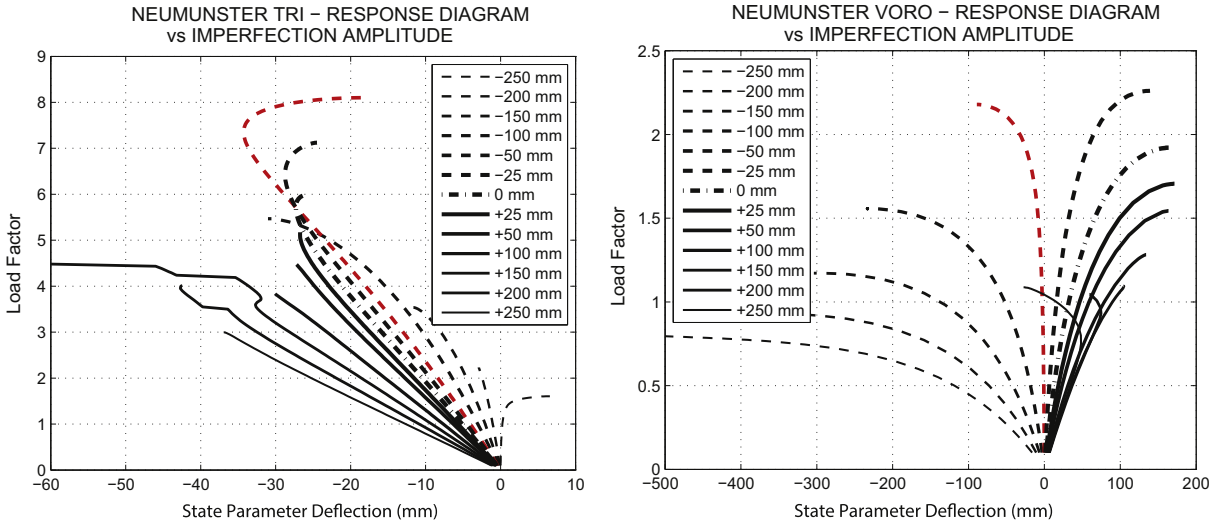

(a) Neumünster Triangular topology

(b) Neumünster statics aware Voronoi-like topology

Fig. 8. Variation of the response diagram with the signed amplitude of the imperfection for the *Neumünster* dataset. On the left the triangular remeshing, on the right our statics aware Voronoi remeshing. The state parameter referred to on the *x* axis is the vertical deflection of the black bullet depicted in Fig. 1.

imperfection shapes taken into account (see Section 3 for details and terminology), the 'worst' is:

1. the first linear eigenmode *LB* for triangular topology (see Figs. 6 (a), (c));
2. either the first linear eigenmode *LB* or the linear static displacement shape *LS* for the quadrilateral topology (see Figs. 6(b), (c) and (a), (d), respectively);
3. the initial buckling shape of the perfect model *NLS* for the Statics Aware Voronoi-like topology (see Figs. 6(a), (b) and (d)).

According to Section 3, other convex combinations of linear eigenmodes have been considered, but in no case any of these has come out as the 'worst' imperfection shape. Unfortunately, in agreement with Bulenda and Knippers [20], from our sensitivity analysis no relationship between imperfection shape and amplitude can be worked out in order to predict the 'worst' imperfection.

6.2. Comparative analysis of 'worst' response diagram vs grid-topology

Fig. 7 shows the 'worst' response diagrams for each grid-topology (i.e. triangular, quadrilateral and Statics Aware Voronoi-like) of each dataset (first column of Table 1). As usual, the term 'worst' response diagram means that it is associated with the imperfect model which produces the lowest load factor.

As expected, triangular grid-shells achieve the highest load factor together with the lowest deformation (see Figs. 7(a) and (b)). As already outlined in Sections 1 and 6.1, the triangular topology is together the strongest as well as the most stiff, to such an extent that it does not require any stiffening device.

On the contrary, almost all of the polygonal grid-shells (i.e. quadrilateral and Statics Aware Voronoi-like) exhibit a very much pronounced softening behavior prior to collapse. They fail when a local maximum is reached along the primary equilibrium path, but by then they have undergone extremely high (totally unsatisfactory) forerunner displacements. Roughly speaking, they behave like thick equivalent continuous shells made of a 'squashy' material (i.e. with low equivalent Young modulus), according to the analytical results of Tonelli [18]. It is worth noticing that this happens irrespective of the regularity of the underlying surface, i.e. there is no distinction between regular datasets such as Neumünster and British Museum and free-form datasets such as Aquadom and Lilium (just compare the scale of the horizontal axis in Figs. 7 (a), (b) and (d)). These huge displacements point out the need for the adoption of an appropriate stiffening method, aimed at reducing the flexibility.

Indeed, polygonal lattice shells exhibit a proper shell behavior only when a suitable stabilizing system is introduced. Usually a bracing cable system is used that caters for the shear forces to be transferred by membrane action, whereas transverse diaphragms might be added in order to provide for the double curvature to be maintained [17].

Eventually, as already pointed out in Section 6.1, the Statics Aware Voronoi Remeshing becomes very effective for architectural free-form surfaces with a high height-to-span ratio (i.e. *Aquadom* and *Lilium Tower* datasets). Indeed, it achieves buckling factors which are on average twice as much as those yielded by equivalent quadrilateral state-of-the-art grid-shells (see Figs. 7(c) and (d)). This excellent result is due both to the innate adaptivity of the Voronoi diagram and to the *'statics awareness'* introduced by Pietroni et al. [1].

6.3. Response diagram vs imperfection amplitude

Fig. 8 illustrates the variation of the response diagram with the signed amplitude of the imperfection for the Neumünster dataset. For the sake of brevity, only the triangular and Statics Aware Voronoi-like topologies are reported with reference to their 'worst' imperfection shape (i.e. the *LS* and *NLS* imperfections, respectively – see Fig. 6(a)).

It is evident that there is no straightforward correlation between the imperfection amplitude and the shape of the response diagram. It is also worth mentioning that GSA [21] works in load control, which in turn means that it is not able to follow the post-buckling behavior (e.g. also the potential bifurcation point of the triangular pattern). A correlation is instead spotted between the trend of the diagrams of Fig. 8 and those of Fig. 6(a). In particular, the cusp points of Fig. 6(a) correspond to a sensible snap-back and an almost infinite slope in the corresponding response diagrams of Figs. 8(a) and (b), respectively. In so doing, the cusp points of Fig. 6(a) can be regarded as 'boundary lines' (red lines in Fig. 8) in the response diagram *vs* imperfection amplitude graphs of Fig. 8.

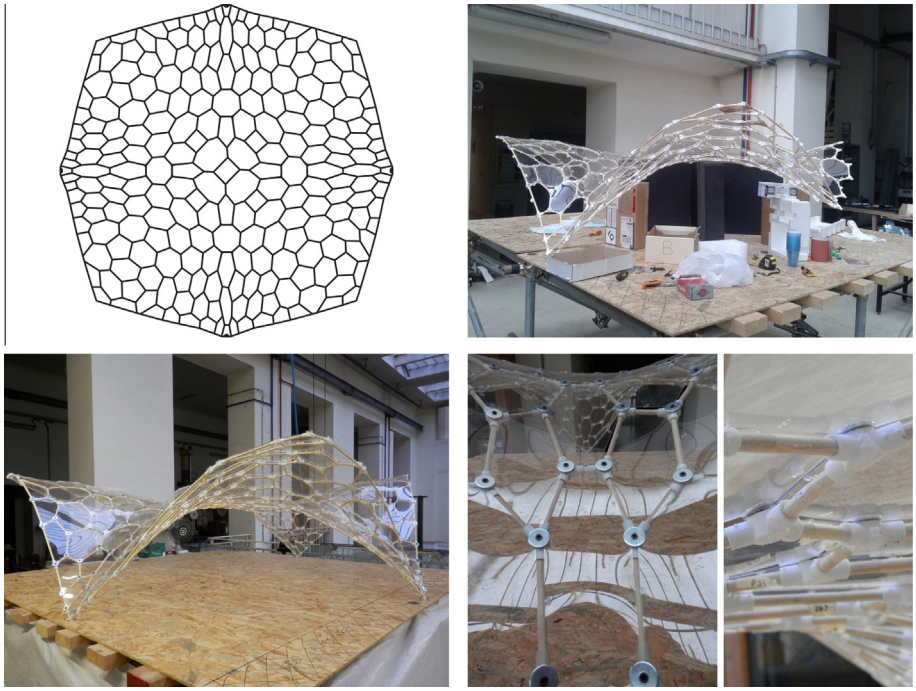

Fig. 9. The geometry of the Statics Aware Voronoi Grid-Shell mock-up.

Table 2
Statistics on the mock-up.

	Beams	Joints	Faces	Washers	Screws
Number	697	231	465	227	243
Material	Mild fir	ABS	PET	Iron	Iron
ρ (kg m^{-3})	400	1050	1400	7750	7750
M_{tot} (kg)	1.5	1.6	7.2	2.5	0.3
M_{tot} (kg)	13.1				

Eventually, the triangular topology displays a rather linear behavior up to collapse (or up to the 80% of the collapse load at least) on average. On the contrary, the Statics Aware Voronoi-like topology exhibits a sensible softening behavior along the loading process, that intensifies as the imperfection amplitude grows.

Unfortunately, there are no evident rules on how to state in advance the load–deflection relation for a whatsoever imperfect structure. Then the engineer has to undergo all the efforts of a thorough imperfection sensitivity analysis, as the response diagram shape affects the safety of the structure.

7. Statics-Aware Voronoi mock-up

A mock-up of Statics Aware Voronoi Grid-Shell has been built at the Department D.E.S.T.e.C. of the University of Pisa, with overall dimensions $(2.4 \times 2.4 \times 0.7)$ m and composed of 465 joints, 697 beams and 231 panels (see Fig. 9 and Table 2 for statistics).

The joints were 3D printed, the timber beams manually cut and the P.E.T. panels laser cut. All the geometry was digitally handled by means of Rhinoceros [47], in particular using its plug-in RhinoScript for automating some procedures. During the assembling phase (lasted 17 days) temporary 'scaffoldings' were needed until the structure was completed and could bear its own weight (see Fig. 9).

8. Conclusions

This paper tackles the problems of the assessment of the structural performance of a novel hex-dominant remeshing pattern for free-from grid-shells: the *Statics Aware Voronoi Remeshing* scheme introduced by Pietroni et al. [1].

The basic intuition for the generation of the geometry is to lay out the beams network along the edges of an Anisotropic Centroidal Voronoi tessellation of the surface, where the metric used is not the Euclidean metric but that induced by the stress tensor over the surface under dead load.

In order to assess their structural capabilities we have carried out a systematic comparative analysis between them and equivalent state-of-the-art competitors (i.e. grid-shells with triangular and quadrilateral topology). To this aim, we have performed extensive investigations through numerical geometrically non-linear analyses. The results we have obtained show that, at least with respect to the specific conditions addressed (i.e. dead loading, rigid joints, pinned boundary, etc.), our free-form Statics Aware Voronoi Grid-Shells are not only aesthetically pleasing but also statically efficient. Obviously they cannot be as efficient as the triangular grid-shells, but they turn out to be twice as effective as their equivalent state-of-the-art quadrilateral competitors. Therefore they may indeed represent a valid alternative for the design of modern grid-shells, especially if the underlying surface is free-form. In particular we have observed that the bigger the irregularity of the underlying surface, the better the structural performances of our Statics Aware Voronoi Grid-Shells thanks to the *statics awareness* supplied by the statically driven metric.

This indeed holds true when the Statics Aware Voronoi Grid-Shells are subject to uniform load cases (e.g. gravity load). On the other hand further research should be carried out in order to assess their effectiveness under different load conditions. In particular anti-metric load cases are envisaged to be extremely detrimental because, as it stands, the Statics Aware Voronoi Remeshing algorithm generates optimal grid-shells with respect to symmetric loading only.

These situations are exactly those in which a prospective stiffening device should kick in, bringing about much needed stiffness. The analysis of such a complex and detailed device is out of the scope of the present study and need to be addressed separately.

Also, to this respect, the stiffness of the joints plays a very important role on the overall behavior of the grid-shell. Generally speaking a grid-shell with all pinned nodes is a mechanism whereas the same grid-shell with rigid joints usually yields the best performances. Nevertheless seldom rigid joints can be achieved in practice and therefore a systematic study would be required in order to assess the effect of the stiffness of the joints over the grid-shell behavior. Again, the analysis of such a delicate matter requires extensive research and as such is clearly out of the scope of the present work.

A thorough imperfection sensitivity analysis has also been carried out. We have found out that the 'worst' imperfection shape is topology-dependent, i.e. it varies with the remeshing pattern even if the underlying surface is kept constant. In particular, the initial buckling shape proposed by Schneider [25,35] under the name of 'quasi-collapse-affine' imperfection seems to be the most unfavorable imperfection for the Statics Aware Voronoi Grid-Shells. Additionally, although less sensitive to imperfections than shells, the reduction of the buckling load might be very high also for grid-shells. Specifically, the stiffer they are the higher their collapse load abatement is.

In particular, the failure load of imperfect triangular grid-shells can be even a quarter of the thoretical value, Statics Aware Voronoi Grid-Shells can have their buckling load halved whereas quadrilateral grid-shells are usually the least sensitive with a maximum fall of 35% (see Fig. 6). Again, these results hold true for grid-shells subject to uniform loading only and hence further research should be carried out to extend them to different load conditions (e.g. antimetric loading).

From a geometrical and pragmatic standpoint, Statics Aware Voronoi meshes have twice the number of vertices with respect to statically equivalent quadrilateral meshes (see Section 5.2), but at the same time all vertices have valence three (see Table 1), thus they are competitive from the feasibility viewpoint too.

At this stage of development the Statics Aware Voronoi Remeshing algorithm does not yield planar faces, thus it is not directly applicable to the design of glass-covered grid-shells. Nevertheless with further focused research we are confident that a face single curvature constraint could be implemented. This in turn would pave the way for the use of rigid cladding materials such as cold-bent glass [48–50], GRP, GRC, etc. For further details about planarity of the faces and geometric aspects, the reader is referred to [1].

References

[1] Pietroni N, Tonelli D, Puppo E, Froli M, Scopigno R, Cignoni P. Statics aware grid shells. Comput Graph Forum 2015;34(2):627–41. http://dx.doi.org/10.1111/cgf.12590.

[2] Koiter W. On the stability of elastic equilibrium. NASA technical translation, National Aeronautics and Space Administration; 1967.

[3] Hutchinson JW. Imperfection sensitivity of externally pressurized spherical shells. J Appl Mech 1967;34:49–55.

[4] Gioncu V. Buckling of reticulated shells: state-of-the-art. Int J Space Struct 1995;10:1–46.

[5] Timoshenko SP, Gere JM. Theory of elastic stability. McGraw-Hill classic textbook reissue, New York: McGraw-Hill; 1988. 1961, reprint. Originally published: 2nd ed. New York: McGraw-Hill, 1961. (Engineering societies monographs).

[6] Weingarten VI, Seide P, Peterson JP. Buckling of thin-walled circular cylinders. Tech. rep., NASA; 1968.

[7] Wright DT. Membrane forces and buckling in reticulated shells. J Struct Div 1965;91(1):173–202.

[8] Forman SE, Hutchinson JW. Buckling of reticulated shell structures. Int J Solids Struct 1970;6(7):909–32. doi: http://dx.doi.org/10.1016/0020-7683(70)90004-1.

[9] Sumec J, Zingali A. A study of the influence of initial shape imperfections on the stability of lattice shells by direct and shell analogy method. Int J Space Struct 1987;2:223–30.

[10] Adriaenssens S, Block P, Veenendaal D, Williams C, editors. Shell structures for architecture: form finding and optimization. London: Taylor and Francis – Routledge; 2014.

[11] Malek S, Williams CJK. Structural implications of using cairo tiling and hexagons in gridshells. In: Proceedings of the international association for shell and spatial structures (IASS) symposium 2013 – "Beyond the Limits of Man", Wroclaw, Poland; 2013.

[12] Schlaich J, Schober H. Glass-covered lightweight spatial structures; 1994. p. 1–27.

[13] Schlaich J, Schober H. Glass-covered grid-shells. Struct Eng Int: J Int Assoc Bridge Struct Eng (IABSE) 1996;6(2):88–90.

[14] Schlaich J, Schober H. Glass roof for the hippo house at the berlin zoo. Struct Eng Int: J Int Assoc Bridge Struct Eng (IABSE) 1997;7(4):252–4.

[15] Glymph J, Shelden D, Ceccato C, Musse J, Schober H. A parametric strategy for free-form glass structures using quadrilateral planar facets. Automat Construct 2004;13:187–202.

[16] Liu Y, Pottmann H, Wallner J, Yang Y-L, Wang W. Geometric modeling with conical meshes and developable surfaces. ACM Trans Graph 2006;25:681–9.

[17] Schlaich J, Schober H. Design principles of glass roofs. In: Proceedings of the international symposium on lightweight structures in civil engineering, Warsaw, Poland; 2002. p. 815–27.

[18] Tonelli D. Statics aware voronoi grid-shells. Ph.D. thesis, University of Pisa; 2014.

[19] Jiang C, Wang J, Wallner J, Pottmann H. Freeform honeycomb structures. Comput Graph Forum 2014;33(5). http://dx.doi.org/10.1111/cgf.12444.

[20] Bulenda T, Knippers J. Stability of grid shells. Comput Struct 2001;79(12):1161–74. doi: http://dx.doi.org/10.1016/S0045-7949(01)00011-6.

[21] Oasys Software. GSA version 8.6 reference manual. Arup, 13 Fitzroy Street London; 2012.

[22] Schmidt H. Stability of steel shell structures: general report. J Construct Steel Res 2000;55(13):159–81. doi: http://dx.doi.org/10.1016/S0143-974X(99)00084-X.

[23] Dinkler D, Pontow J. A model to evaluate dynamic stability of imperfection sensitive shells. Comput Mech 2006;37(6):523–9. http://dx.doi.org/10.1007/s00466-005-0729-7.

[24] Ewert E, Schweizerhof K, Vielsack P. Measures to judge the sensitivity of thin-walled shells concerning stability under different loading conditions. Comput Mech 2006;37(6):507–22. http://dx.doi.org/10.1007/s00466-005-0733-y.

[25] Schneider W, Timmel I, Hhn K. The conception of quasi-collapse-affine imperfections: a new approach to unfavourable imperfections of thin-walled shell structures. Thin-Wall Struct 2005;43(8):1202–24. doi: http://dx.doi.org/10.1016/j.tws.2005.03.003.

[26] Deml M, Wunderlich W. Direct evaluation of the worst imperfection shape in shell buckling. Comput Methods Appl Mech Eng 1997;149(14):201–22. Containing papers presented at the symposium on advances in computational mechanics. doi: http://dx.doi.org/10.1016/S0045-7825(97)00055-8.

[27] Ho D. The influence of imperfections on systems with coincident buckling loads. Int J Non-Linear Mech 1972;7(3):311–21. doi: http://dx.doi.org/10.1016/0020-7462(72)90053-4.

[28] Greiner R, Derler P. Effect of imperfections on wind-loaded cylindrical shells. Thin-Wall Struct 1995;23(14):271–81. Buckling strength of imperfection-sensitive shells. doi: http://dx.doi.org/10.1016/0263-8231(95)00016-7.

[29] Lindgaard E, Lund E, Rasmussen K. Nonlinear buckling optimization of composite structures considering worst shape imperfections. Int J Solids Struct 2010;47(2223):3186–202. doi: http://dx.doi.org/10.1016/j.ijsolstr.2010.07.020.

[30] CEN. Eurocode 3: design of steel structures. Part 1–6: Strength and stability of shell structures, CEN; 2007. <https://law.resource.org/pub/eur/ibr/en.1993.1.6.2007.html>.

[31] Graciano C, Casanova E, Martnez J. Imperfection sensitivity of plate girder webs subjected to patch loading. J Construct Steel Res 2011;67(7):1128–33. doi: http://dx.doi.org/10.1016/j.jcsr.2011.02.006.

[32] Kristani N, Korelc J. Optimization method for the determination of the most unfavorable imperfection of structures. Comput Mech 2008;42(6):859–72. http://dx.doi.org/10.1007/s00466-008-0288-9.

[33] Song C, Teng J, Rotter J. Imperfection sensitivity of thin elastic cylindrical shells subject to partial axial compression. Int J Solids Struct 2004;41(2425):7155–80. doi: http://dx.doi.org/10.1016/j.ijsolstr.2004.05.040.

[34] Schneider W, Brede A. Consistent equivalent geometric imperfections for the numerical buckling strength verification of cylindrical shells under uniform external pressure. Thin-Wall Struct 2005;43(2):175–88. doi: http://dx.doi.org/10.1016/j.tws.2004.08.006.

[35] Schneider W. Stimulating equivalent geometric imperfections for the numerical buckling strength verification of axially compressed cylindrical steel shells. Comput Mech 2006;37(6):530–6. http://dx.doi.org/10.1007/s00466-005-0728-8.

[36] Du Q, Faber V, Gunzburger M. Centroidal voronoi tessellations: applications and algorithms. SIAM Rev 1999;41(4):637–76. http://dx.doi.org/10.1137/S0036144599352836.

[37] Corsini M, Cignoni P, Scopigno R. Efficient and flexible sampling with blue noise properties of triangular meshes. IEEE Trans Visual Comput Graph 2012;18(6):914–24.

[38] Valette S, Chassery J-M. Approximated centroidal voronoi diagrams for uniform polygonal mesh coarsening. Comput Graph Forum 2004;23(3):381–9. http://dx.doi.org/10.1111/j.1467-8659.2004.00769.x.

[39] RFR-Paris. Neumünster abbey glazing, neumünster luxembourg; 2003.

[40] Williams CJK. The analytic and numerical definition of the geometry of the british museum great court roof. In: Proceedings of the third international

conference on mathematics & design, M&D, Deakin Unversity, Geelong, Australia; 2001. p. 434–40.
[41] Vouga E, Höbinger M, Wallner J, Pottmann H. Design of self-supporting surfaces. ACM trans. graphics proc. SIGGRAPH; 2012.
[42] do Carmo MP. Differential geometry of curves and surfaces. Prentice Hall; 1976.
[43] Alexandrov AD. On the works of S.E. Cohn-Vossen. Upsehi Matem Nauk 1947;2 (3(19)):107–41.
[44] Calladine CR. Theory of shell structures. Cambridge, Cambridgeshire, New York: Cambridge University Press; 1983. includes index.
[45] Rayleigh L. On Bells, The London. Edinburgh Dublin Philos Mag J Sci 1890 (5). http://www.hibberts.co.uk/rayleigh.htm.
[46] Thompson J, Hunt G. Elastic instability phenomena. 1st ed. New York, NY, USA: John Wiley & Sons, Inc.; 1984.
[47] Becker M, Golay P. Rhino NURBS 3D Modeling, no. v. 1, New Riders; 1999.
[48] Belis J, Inghelbrecht B, Van Impe R, Callewaert D. Experimental assessment of cold-bent glass panels. Glass Perform Days, Tamglass 2007;1:115–7.
[49] Eekhout M, Staaks D. Cold deformation of glass. Glass Perform Days 2007.
[50] Vakar L, Gaal M, Bendable Cold. Laminated glass – new possibilities in design. Struct Eng Int (SEI) 2004;14(2):95–7.